The Astrophysical Journal Letters, 946:L37 (8pp), 2023 April 1 https://doi.org/10.3847/2041-8213/acc2bb

The Undiscovered Ultradiffuse Galaxies of the Local Group

Oliver Newton[1,2], Arianna Di Cintio[3,4], Salvador Cardona–Barrero[3,4], Noam I. Libeskind[5,2], Yehuda Hoffman[6], Alexander Knebe[7,8,9], Jenny G. Sorce[5,10,11], Matthias Steinmetz[5], and Elmo Tempel[12,13]
[1] Center for Theoretical Physics, Polish Academy of Sciences, al. Lotników 32/46 Warsaw, Poland; onewton@cft.edu.pl
[2] Univ. Lyon, Univ. Claude Bernard Lyon 1, CNRS, IP2I Lyon/IN2P3, IMR 5822, F-69622, Villeurbanne, France
[3] Universidad de La Laguna. Avda. Astrofísico Fco. Sánchez, La Laguna, Tenerife, Spain; adicintio@iac.es
[4] Instituto de Astrofísica de Canarias, Calle Via Láctea s/n, E-38206 La Laguna, Tenerife, Spain
[5] Leibniz-Institut für Astrophysik Potsdam, An der Sternwarte 16, D-14482 Potsdam, Germany
[6] Racah Institute of Physics, Hebrew University, Jerusalem, 91904, Israel
[7] Departamento de Física Teórica, Módulo 15, Facultad de Ciencias, Universidad Autónoma de Madrid, E-28049 Madrid, Spain
[8] Centro de Investigación Avanzada en Física Fundamental (CIAFF), Facultad de Ciencias, Universidad Autónoma de Madrid, E-28049 Madrid, Spain
[9] International Centre for Radio Astronomy Research, University of Western Australia, 35 Stirling Highway, Crawley, Western Australia 6009, Australia
[10] Univ. Lille, CNRS, Centrale Lille, UMR 9189 CRIStAL, F-59000 Lille, France
[11] Univ. Paris-Saclay, CNRS, Institut d'Astrophysique Spatiale, F-91405 Orsay, France
[12] Tartu Observatory, University of Tartu, Observatooriumi 1, 61602 Tõravere, Estonia
[13] Estonian Academy of Sciences, 10130 Kohtu 6, Tallinn, Estonia
Received 2023 January 5; revised 2023 March 6; accepted 2023 March 9; published 2023 March 30

Abstract

Ultradiffuse galaxies (UDGs) are attractive candidates to probe cosmological models and test theories of galaxy formation at low masses; however, they are difficult to detect because of their low surface brightness. In the Local Group a handful of UDGs have been found to date, most of which are satellites of the Milky Way and M31, and only two are isolated galaxies. It is unclear whether so few UDGs are expected. We address this by studying the population of UDGs formed in hydrodynamic constrained simulations of the Local Group from the HESTIA suite. For a Local Group with a total enclosed mass $M_{\rm LG}(<2.5\,{\rm Mpc}) = 8\times10^{12}\ {\rm M}_\odot$, we predict that there are 12 ± 3 isolated UDGs (68% confidence) with stellar masses $10^6 \leqslant M_*/{\rm M}_\odot < 10^9$, and effective radii $R_{\rm e} \geqslant 1.5$ kpc, within 2.5 Mpc of the Local Group, of which 2^{+2}_{-1} (68% confidence) are detectable in the footprint of the Sloan Digital Sky Survey (SDSS). Accounting for survey incompleteness, we find that almost the entire population of UDGs in the Local Group field would be observable in a future all-sky survey with a depth similar to the SDSS, the Dark Energy Survey, or the Legacy Survey of Space and Time. Our results suggest that there is a population of UDGs in the Local Group awaiting discovery.

Unified Astronomy Thesaurus concepts: Dwarf galaxies (416); Galaxy formation (595); Galaxy interactions (600); Local Group (929); Low surface brightness galaxies (940); Luminosity function (942)

1. Introduction

Hierarchical models of galaxy formation predict the emergence of a large population of low-mass galaxies. Typically, they are dominated by sizable dark matter (DM) components that make them useful as discerning probes of cosmological models. The most valuable galaxies for this purpose are those that contain little baryonic material, which is dispersed throughout a large volume. Such faint and extended galaxies were first characterized by Sandage & Binggeli (1984), and a handful of additional systems were described subsequently (Impey et al. 1988; Thompson & Gregory 1993; Jerjen et al. 2000; Conselice et al. 2003; Mieske et al. 2007; De Rijcke et al. 2009; Penny et al. 2009). More recently, studies of this subpopulation of galaxies have been invigorated by the discovery of hundreds of systems in several different environments: within clusters of galaxies such as Coma, Virgo, and Fornax (Koda et al. 2015; van Dokkum et al. 2015; Martínez-Delgado et al. 2016; Román & Trujillo 2017); in galaxy groups (Trujillo et al. 2017); and in the field in between (e.g., Leisman et al. 2017). These extended objects have stellar masses and magnitudes typical of bright dwarf galaxies ($M_* = 10^{6-9}\,{\rm M}_\odot$ and $M_{\rm V} < -8$, respectively); however, they are significantly larger, with sizes approaching those of massive galaxies such as the Milky Way. As a result they have very low surface brightness, usually between $\mu_{\rm e} = 24$ and 28 mag arcsec^{-2}, earning them the sobriquet "ultradiffuse galaxies" (UDGs).

The circumstances leading to the emergence of such diffuse galaxies are not understood fully and several scenarios have been proposed to explain their formation. These are divided broadly into two main categories: (i) internal processes that drive stars toward the outer regions of the galaxy, as could happen in haloes with high spin (Amorisco & Loeb 2016), and during episodes of powerful stellar feedback (Di Cintio et al. 2017; Chan et al. 2018; Cardona-Barrero et al. 2023); and (ii) the disturbance caused by external mechanisms such as stripping and tidal heating (Carleton et al. 2019; Jiang et al. 2019; Tremmel et al. 2020; Benavides et al. 2021), and galaxy mergers (Wright et al. 2021). A compelling test of these proposals requires a large sample of UDGs, the catalog of which has grown rapidly in recent years because of advances in instrumentation and observational techniques. However, UDGs remain challenging to detect so their census in the nearby universe is likely far from complete.

Similarly, the census of dwarf galaxies within the Local Group is also incomplete (Garrison-Kimmel et al. 2014; Newton et al. 2018; Nadler et al. 2019; Drlica-Wagner et al. 2020; Fattahi et al. 2020b). Using the Di Cintio et al. (2017)

definition of UDGs, only eight Local Group galaxies satisfy the criteria: And II, And XIX, And XXXII, Antlia II, Crater II, Sagittarius dSph, WLM, and IC1613 (Collins et al. 2013; Kirby et al. 2014; Torrealba et al. 2016; Caldwell et al. 2017, see also McConnachie 2012 for observational data). Of these, six are satellites of the Milky Way and M31 and only IC1613 and WLM are found "in the field" of the Local Group, i.e., they are outside the virial radii of the Milky Way and M31, which we take to be 230 and 275 kpc, respectively. It is unclear whether the dearth of UDGs in the field of the Local Group arises primarily from environmental influences that prevent most galaxies from becoming UDGs, or if observational limitations are the main obstacle impeding their detection. Indeed, if such a UDG population exists it would be partly obscured by the foreground of Milky Way stars and the background of other galaxies, making it difficult to detect with current instruments. Therefore, in this Letter we use high-resolution simulations to quantify the number of UDGs that we expect to find in the field within 2.5 Mpc of the Local Group, and study their potential detectability in current and forthcoming surveys.

2. Methodology

To estimate the size and properties of the population of UDGs in the field of the Local Group we require simulations that self-consistently model the formation and evolution of galaxies in this environment. The HESTIA suite does this (Libeskind et al. 2020), and consists of 13 zoom-in simulations of Local Group analogs that were run with the AREPO moving mesh code (Springel 2010) and the AURIGA galaxy formation model (Grand et al. 2017). Using estimates of the peculiar velocity field derived from observations (Tully et al. 2013), the initial conditions are constrained to reproduce the major gravitational sources in the neighborhood of the Local Group. Consequently, at $z = 0$ the Local Group analogs are embedded in large-scale structure that is consistent with the observations when assuming the Λ+cold dark matter (ΛCDM) cosmological model (see, e.g., Hoffman & Ribak 1991; Doumler et al. 2013; Sorce et al. 2016).

The Local Group analogs are simulated at "low" and "intermediate" resolution in a Planck Collaboration et al. (2014) cosmology. Three were resimulated at higher resolution using ~200M DM particles in a high-resolution region consisting of two overlapping spherical volumes with radii of $2.5\,h^{-1}$ Mpc, each centered on the Milky Way and M31 analogs at $z = 0$. The spatial resolution achieved is 177 pc, and the effective masses of the DM and gas particles are $M_{\rm DM} = 2 \times 10^5\,{\rm M}_\odot$ and $M_{\rm gas} = 2.2 \times 10^4\,{\rm M}_\odot$, respectively. The simulations are labeled `09_18`, `17_11`, and `37_11`, after the initial seed used, and their physical properties can be found in Libeskind et al. (2020, Table 1). We use the Amiga Halo Finder (AHF) algorithm (Gill et al. 2004; Knollmann & Knebe 2009) to identify and characterize gravitationally bound structures in the simulations.

In the AURIGA model the star particles represent simple stellar populations of a given age, mass, and metallicity. Upon creation they are initialized using a Chabrier (2003) initial mass function, and the mass that is subsequently lost due to stellar evolution is calculated using the yield curves from Portinari et al. (1998) and Karakas (2010). The photometric properties of each star particle are computed using the Bruzual & Charlot (2003) stellar population synthesis model while neglecting the effects of dust attenuation. Consequently, the stellar populations may be as much as 0.75 mag brighter in the V and r bands that are of interest in this Letter than they would be if dust attenuation was accounted for. However, we note that the isolated, low-mass galaxies in HESTIA experience minimal star formation activity at $z = 0$, so we expect that including dust attenuation would produce only a small effect.

2.1. UDG Selection Criteria

The UDGs we study here are drawn from the population of Local Group field haloes in each high-resolution simulation. They are located within 2.5 Mpc of the center of the Local Group at $z = 0$ and are outside R_{200} (the radius of the sphere enclosing a mean matter density of $\rho(<R_{200}) = 200 \times \rho_{\rm crit}$, where $\rho_{\rm crit}$ is the critical density for closure) of all haloes that are at least as massive as the Milky Way analog. We select UDGs from the field haloes by applying criteria similar to those described in Di Cintio et al. (2017): (i) the candidate has a total stellar mass, $M_* \leqslant 10^9\,{\rm M}_\odot$; (ii) it has a two-dimensional effective radius, which contains half of the total luminosity of the system, $R_{\rm e} \geqslant 1.5$ kpc; and (iii) it has effective surface brightness, $\mu_{\rm e} = \mu(< R_e) \geqslant 24$ mag arcsec^{-2}. Both $R_{\rm e}$ and $\mu_{\rm e}$ depend on the luminosity of the galaxy, which we compute in the r band while ignoring the effects of dust attenuation. We calculate these values by orienting the galaxy so that the gas disk is face-on to the observer and project the star particles into the plane of the disk. When a galaxy has no identifiable gas disk we take the simulation z-axis to be normal to the disk plane. To minimize the effects of the limited simulation resolution we also require that each UDG has at least 50 star particles. This is equivalent to imposing an effective minimum stellar mass of approximately $\log_{10}(M_*/{\rm M}_\odot) = 6.05^{+0.09}_{-0.10}$ (68% scatter).

In Figure 1, we show two of the key selection criteria applied to the simulated field galaxies. The filled symbols show UDGs that satisfy the modified Di Cintio et al. (2017) criteria described above, and have stellar masses in the range $M_* = [10^6, 10^9]\,{\rm M}_\odot$. Larger markers indicate galaxies that are closer to one of the hosts. Generally, the largest UDGs are found in close proximity to the Milky Way and M31 analogs. There are 24, 15, and 11 UDGs in the fields of the `09_18`, `17_11`, and `37_11` simulations, respectively. A detailed analysis of their formation histories will be conducted in a companion paper (S. Cardona-Barrero et al. 2023, in preparation).

In Figure 2, we show the distribution of the UDGs in one representative high-resolution simulation (`17_11`; chosen arbitrarily). This shows the projected DM, gas, and stellar density in a spherical region with a radius of 2.5 Mpc centered on the midpoint of the Milky Way and M31 analogs. The distribution of UDGs throughout the volume is not uniform: at small distances from the center of the Local Group the UDGs cluster close to R_{200} of the Milky Way and M31 analogs, and in the other simulations they congregate nearer to the splashback radii of the hosts (as defined in Diemer 2021). However, at larger distances from the center of the Local Group the UDGs are affiliated preferentially with the large structures that compose the Local Group analog and the filaments and sheets that deliver matter to it.

3. Results

The total number of field galaxies, $N_{\rm field,tot}$, within 2.5 Mpc scales with the total enclosed mass, $M_{\rm LG}(< 2.5\,{\rm Mpc})$, of the

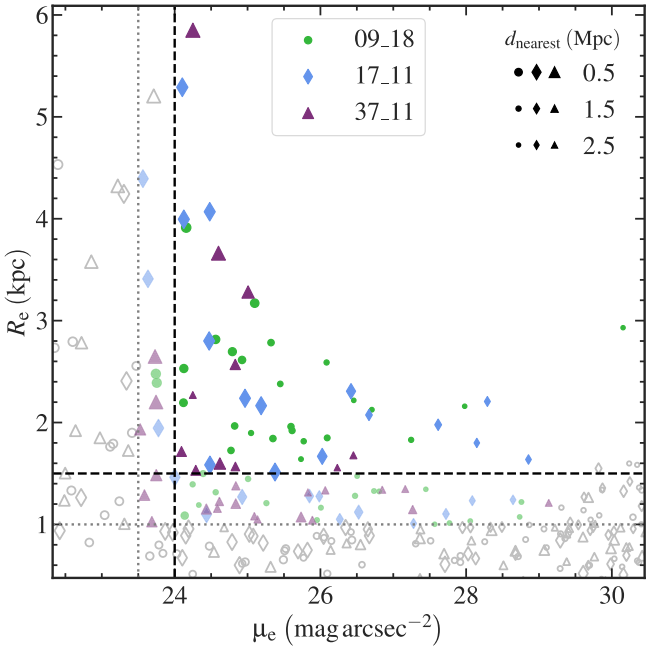

Figure 1. The two-dimensional effective radius, $R_{\rm e}$, as a function of the r-band effective surface brightness, $\mu_{\rm e}$, of the field UDGs in the three high-resolution HESTIA simulations. The size of each marker is inversely proportional to the distance to the nearest host galaxy. The dashed lines show two of our selection criteria applied to the field haloes in the simulations. The galaxies that satisfy all of the selection criteria described in Section 2.1 are plotted with filled symbols, while unfilled symbols show the rest of the field galaxies. The faint filled symbols show galaxies that satisfy less stringent selection criteria (dotted lines) that are often used in the literature.

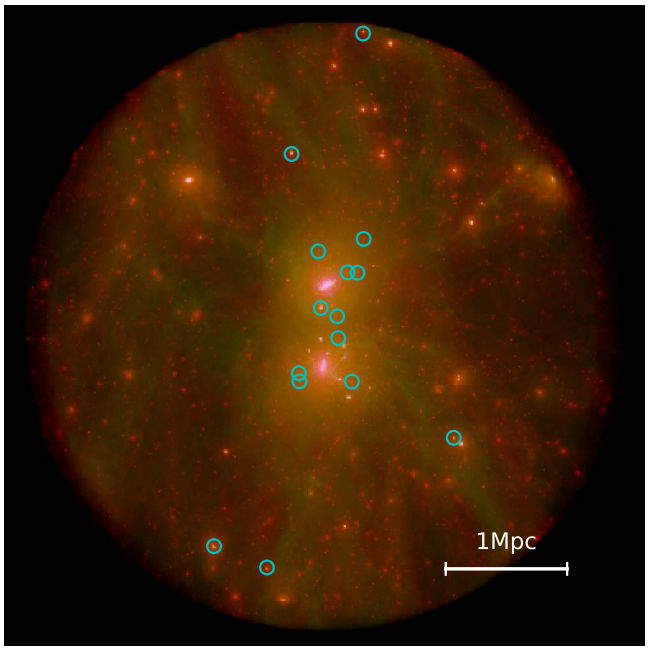

Figure 2. The projected mass-weighted densities of DM (red), gas (green), and stars (white) within 2.5 Mpc of the Local Group in the 17_11 simulation. The two bright galaxies at the center are the analogs of the Milky Way and M31 and we mark the projected positions of the UDGs with light-blue circles.

Local Group (see Fattahi et al. 2020a). This differs by a factor of 1.6 between the least- and most-massive simulations and causes $N_{\rm field,tot}$ to vary between 50 and 79 (see Table 1). The total number of UDGs, $N_{\rm UDG,tot}$, in each simulation varies

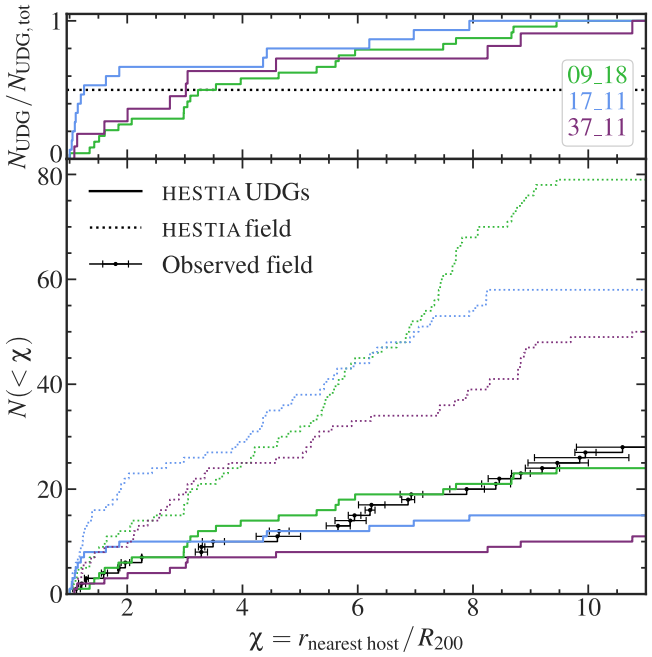

Figure 3. Lower panel: the whole-sky radial cumulative distributions of UDGs (solid lines) and all field galaxies (dotted lines) with stellar masses, $10^6 \leqslant M_*/\,{\rm M}_\odot < 10^9$, as a function of the distance to the nearest host galaxy, $r_{\rm nearest}$, normalized to the host galaxy's R_{200}. We overlay the incomplete census of observed field galaxies as points with error bars showing the 68% distance uncertainties (using data compiled by McConnachie 2012). Upper panel: the cumulative distribution function of the UDGs in each HESTIA simulation. To aid the eye, we mark the 50% threshold with a horizontal dotted line.

Table 1
The $z = 0$ Properties of the Three Simulations

Simulation	$M_{\rm LG}$ (10^{13} M$_\odot$)	$N_{\rm field,tot}$	$N_{\rm UDG,tot}$
09_18	1.23	79	24
17_11	1.03	58	15
37_11	0.77	50	11

Note. We provide the total enclosed mass, $M_{\rm LG}$, the number of field galaxies, $N_{\rm field,tot}$, and the number of UDGs, $N_{\rm UDG,tot}$, with $10^6 \leqslant M_*/{\rm M}_\odot \leqslant 10^9$ within 2.5 Mpc of the midpoint of the primary haloes. Note the different observer position to that in Figure 3.

between 11 and 24, and accounts for 22%–30% of the total population of field galaxies in the stellar mass range $10^6 \leqslant M_*/\,{\rm M}_\odot \leqslant 10^9$. This is consistent with the results from the ROMULUSC galaxy cluster simulation that shows that a large fraction of low-mass galaxies at $z = 0$ are UDGs (Tremmel et al. 2020).

In Figure 3, we show the cumulative radial distributions of field galaxies and field UDGs in each high-resolution volume with respect to the nearest host galaxy analog at $z = 0$. We also overlay the incomplete census of observed field galaxies in the stellar mass range described above. Their distances with respect to the Milky Way and M31 are calculated using the equatorial coordinates and distance moduli compiled in the most recently updated catalog of McConnachie (2012). As we described in Section 1, we exclude galaxies that are within the virial radius of the Milky Way or M31. The observational data are limited by incomplete sky coverage and insufficient sensitivity to low-surface-brightness objects, which partly explains the

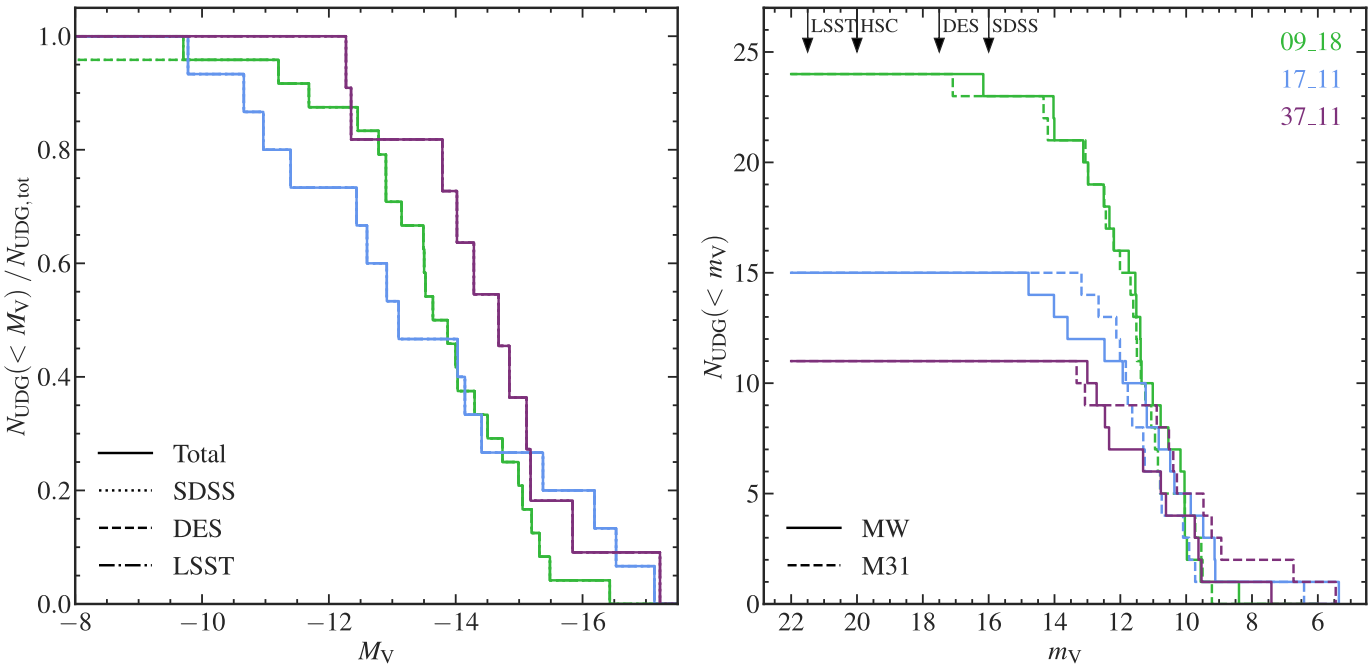

Figure 4. The total luminosity functions of field UDGs within 2.5 Mpc of each high-resolution Local Group simulation in the HESTIA suite. Left panel: we estimate the absolute *V*-band magnitude luminosity functions as a fraction of the total number of UDGs, $N_{UDG,tot}$, likely to be observed in whole-sky SDSS-, DES-, and LSST-like surveys by applying a limiting surface-brightness cut in the *r* band when assuming that the stars in each galaxy are individually resolved (SDSS: 29 mag arcsec^{-2}, DES: 30 mag arcsec^{-2}, LSST: 31 mag arcsec^{-2}). With the exception of the SDSS and DES curves in the `09_18` simulation, the luminosity functions of all surveys overlap with the "Total" luminosity function. Right panel: the cumulative number of field UDGs in the simulations as a function of apparent *V*-band magnitude, m_V. The solid and dashed lines show the luminosity functions measured by observers in the Milky Way and M31 analogs, respectively. The vertical arrows indicate the faintest dwarf galaxies that could be detected in several past and future surveys: SDSS ($m_V = 16$), DES ($m_V = 17.5$), HSC ($m_V = 20$), and LSST ($m_V = 21.5$).

discrepancy between these data and the number of field galaxies we identify in the simulations (see the bottom panel of Figure 3). As we will discuss in Section 3.2, we think that the `17_11` and `09_18` simulations could be 1.25–1.5 times more massive than the Local Group. We expect that this would increase the number of field galaxies we identify in the simulations by a similar factor. Between 62% and 80% of the field UDGs in the simulations are found within 1.5 Mpc of the center of the Local Group, and approximately half are between R_{200} and $3 \times R_{200}$ of the host galaxies (see the upper panel of Figure 3). The latter distance is consistent with the splashback radius defined in Diemer (2021). At larger radii, the UDGs are affiliated preferentially with the filaments and sheets that feed the growth of the Local Group (see also Figure 2). This is in agreement with the results of Fattahi et al. (2020a), who used the APOSTLE simulations to show that most undiscovered dwarf galaxies should lie near the virial boundaries of the primary haloes.

3.1. Total Luminosity Functions

The luminosity functions of the UDGs within 2.5 Mpc of the center of each Local Group analog are shown in Figure 4. All of the UDGs in the HESTIA simulations are as bright as the classical satellite galaxies of the Milky Way ($M_V < -8$); however, they are much more diffuse and are close to the Milky Way and M31, which makes them difficult to detect in wide-area surveys using standard analysis techniques. To estimate how many UDGs could be observable in all-sky surveys with response functions similar to the Sloan Digital Sky Survey (SDSS; Blanton et al. 2017), the Dark Energy Survey (DES; Abbott et al. 2018), and the Legacy Survey of Space and Time (LSST; Ivezić et al. 2019), we apply limiting surface-brightness cuts in the *r* band of 29, 30, and 31 mag arcsec^{-2}, respectively. We choose these with reference to the response function of the SDSS determined by Koposov et al. (2008), and the design sensitivity of the LSST (Laine et al. 2018), both of which bracket the sensitivity of the DES. These limits apply to studies of resolved galaxies, and are several magnitudes deeper than the limits that are achievable in unresolved searches (V. Belokurov 2022, private communication). Under these assumptions few of the HESTIA UDGs are too faint to be detected (Figure 4, left panel). This simplified scenario suggests that almost the entire field UDG population is detectable in all-sky surveys with SDSS-, DES-, and LSST-like surface-brightness limits. In practice, the surface-brightness limits depend on distance such that nearby very-low-surface-brightness galaxies are not observable (see, e.g., Koposov et al. 2008). We find that most of the field UDGs in HESTIA are close to the Milky Way and M31 analogs, so they could be difficult to detect; however, their surface brightnesses are high enough that they are detectable in the surveys.

In the right panel of Figure 4, we plot the apparent *V*-band magnitude luminosity functions of the UDG populations. We generate luminosity functions for an observer located in the Milky Way and M31 analogs; however, there is little difference between them because the distributions of relative distances to the UDGs are similar. The magnitude limits of the surveys are marked with arrows and suggest that, on the basis of apparent magnitude alone, almost the entire UDG population is detectable in SDSS-, DES-, and LSST-like surveys. Taken together, the panels in Figure 4 illustrate that UDGs in the Local Group should be detectable in all extant wide-area surveys. The most significant factors that could limit their detectability are likely to be their inclination with respect to the

observer, which we discuss in Section 3.2; and the obscuration of the sky by the Galactic disk, which we do not model here.

3.2. Mock Luminosity Functions

The HESTIA simulations predict that UDGs exist in the field of the Local Group at $z = 0$ and that a fraction of them are potentially detectable by surveys such as the SDSS. As very few field UDGs have been found to date, this suggests that several await discovery or that current models of galaxy formation do not accurately describe the physics at low masses. One test of this is to estimate how many UDGs we expect to find in the footprints of current surveys such as the SDSS and whether they are, in principle, detectable using existing data sets.

To study this, we construct mock SDSS observations of the population of field UDGs in the three simulations. This requires an understanding of the observational selection function of low-mass galaxies obtained by an algorithmic search of the survey data. Modern approaches to search for low-mass galaxies in wide-area surveys commonly adopt one, or both, of two complementary techniques: (i) matched-filter searches that apply criteria to select samples of stars at a given distance and compare their spatial overdensity with the Galactic foreground (e.g., Koposov et al. 2008; Walsh et al. 2009); and (ii) likelihood-based searches that model the properties of the stellar populations and incorporate observational uncertainties that are specific to the survey, such as the survey depth (e.g., Bechtol et al. 2015; Drlica-Wagner et al. 2015). These are powerful techniques to search large areas of the sky efficiently but they are less sensitive than other methods to find spatially extended and low-surface-brightness galaxies. Approaches such as resolved star searches have been used very effectively to detect nebulous galaxies in small surveys like Hyper Suprime-Cam (HSC; Garling et al. 2020); however, they are impractical for wide-area sky searches. For this reason, in this study we use the selection function obtained by Koposov et al. (2008), who applied a matched-filter search to SDSS data.

Koposov et al. (2008) characterize the efficiency with which their algorithm detects galaxies with sizes up to 1 kpc at distances as far as 1 Mpc from the Sun. They do this using models of galaxies that are less spatially extended and closer than the field UDGs in the HESTIA simulations. Therefore, to apply their approach and estimate the HESTIA UDG detection efficiency in SDSS, we extend to larger effective radii at greater distances from the Milky Way the relationships they calculated for the parameters in their matched-filter algorithms. This means that the detectability of the most distant galaxies could be overestimated because we do not account for star-galaxy confusion that most likely dominates the signal at large distances. Furthermore, we also disregard the effects of dust attenuation on the UDGs, and their possible obscuration by the Milky Way at Galactic latitudes $|b| \leqslant 10^{\circ}$, known as the Zone of Avoidance (ZoA). Our results should therefore be interpreted as an upper bound on the detectability of UDGs in the SDSS footprint when using this search algorithm. Using the analytic form provided by Koposov et al. (2008), the detection efficiencies, ϵ, of the UDGs in the SDSS are given by

$$\epsilon(M_{\rm V},\, \mu) = G(M_{\rm V} - M_{\rm V,lim})G(\mu - \mu_{\rm lim}), \quad (1)$$

where

$$G(x) = \frac{1}{\sqrt{2\pi}} \int_{x}^{\infty} \exp -\frac{t^2}{2}\, dt. \quad (2)$$

We infer the limiting absolute V-band magnitude, $M_{\rm V,lim}$, and the limiting surface brightness, $\mu_{\rm lim}$, at distances greater than 1 Mpc using a linear fit to the relationships in Koposov et al. (2008, Figure 12).

To generate a mock observation, we place an observer at the center of one of the primary haloes. We model the mock survey as a conical volume with an opening angle of 14,555 deg^2, corresponding to the sky coverage of the SDSS, and orient it so that its apex coincides with the observer. To account for the effects of the viewing angle, we assign each UDG a random orientation with respect to the observer and recalculate $R_{\rm e}$ and $\mu_{\rm e}$. UDGs that fail the selection criteria described in Section 2.1 are discarded before the analysis proceeds. Using the relative distances of the UDGs with respect to the observer and the recomputed values of $\mu_{\rm e}$, we calculate ϵ using Equation (1). This represents the probability of detecting each UDG, and we use it to randomly select a set of UDGs that are detectable in the mock survey. As most galaxies have $\epsilon \sim 1$ the effect of the random sampling is small.

We repeat this procedure for 15,000 pointings of the mock survey distributed evenly across the sky, and again for an observer in the second primary halo. We find that 30,000 mock observations in each high-resolution simulation produces results that are well converged. Using these, we compute the medians and 68% scatter of the field UDG luminosity functions that are detectable in SDSS (see Figure 5). From this, in an SDSS-like survey we find one to four UDGs within 2.5 Mpc of the Milky Way analogs with $\mu_{\rm e}$ brighter than 29 mag arcsec^{-2} in the r band. Approximately 44% of the simulated UDGs that are detectable in each mock SDSS observation are misclassified as non-UDGs because of projection effects arising from their orientation with respect to the observer. Only 5% of the mock observations contain at least one simulated UDG that is not detected at all. The projection effects impose the most significant limitation on the discoverability of UDGs in extant surveys. As we showed in Section 3.1, survey incompleteness has only a minimal effect on the number of UDGs that can be found.

As stated earlier, the total number of field galaxies depends strongly on $M_{\rm LG}$, which is different in each HESTIA simulation. To account for this, we rescale the total mass of each simulation to $M_{\rm LG}(<2.5\,{\rm Mpc}) = 8 \times 10^{12}\ {\rm M}_{\odot}$ and adjust the number density of field galaxies according to the enclosed Local Group mass–galaxy number density relationship in Fattahi et al. (2020a). Our choice of the mass enclosed within 2.5 Mpc is motivated by current observational estimates of $M_{\rm LG}(<1\ {\rm Mpc}) = [3,\ 4.75] \times 10^{12}\ {\rm M}_{\odot}$ (Lemos et al. 2021; Carlesi et al. 2022; Hartl & Strigari 2022). We use the mass profiles of the simulated Local Groups to extrapolate these values to an outer radius of 2.5 Mpc and select the average mass. From this, we expect to find 52 ± 7 (68% confidence, CL) field galaxies with stellar masses $10^6 \leqslant M_*/{\rm M}_{\odot} < 10^9$ within 2.5 Mpc of the center of the Local Group. Of these, approximately one-quarter (12 ± 3) are UDGs, and 2^{+2}_{-1} (68% CL) of them should be detectable in a reanalysis of the footprint of the SDSS. Conducting a similar analysis for the DES and LSST using the Koposov et al. (2008) response function with deeper surface-brightness and magnitude limits

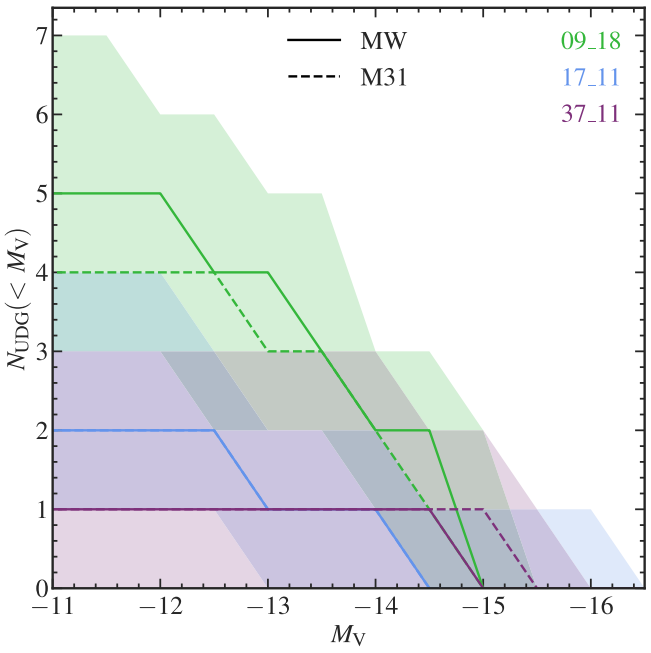

Figure 5. Mock SDSS observations of the population of field UDGs. The solid and dashed lines show the median predictions obtained by observers in the Milky Way and M31 analogs, respectively. The shaded regions represent the 68% scatter in the Milky Way analog luminosity functions over 15,000 mock observations.

(by 1 and 2 mag, for each respective survey), we expect that 3^{+3}_{-2} UDGs are detectable in the combined SDSS+DES footprint, and 4 ± 2 will be detectable in the LSST (see Table 2). Using our selection criteria, no UDGs have been observed in the SDSS footprint to date. Disregarding the effects of dust attenuation, we estimate that the chance that there are no field UDGs detectable in the SDSS footprint is less than 13.1%. In Table 2 we provide the predicted number of field galaxies and UDGs for different choices of $M_{\rm LG}$ and other UDG selection criteria.

4. Discussion and Conclusions

In this Letter, we provide quantitative predictions of the size and luminosity function of the population of isolated UDGs within 2.5 Mpc of the Local Group (which we call "Local Group field UDGs"), and estimate how many could be detectable in dedicated searches of current data sets, and in future surveys. We produce these predictions using the populations of UDGs in the highest-resolution hydrodynamic simulations from the HESTIA suite that are constrained to reproduce the local large-scale structure at $z = 0$. This is the first time that such spatially extended galaxies have been simulated self-consistently in such environments (see Figures 1 and 2). To obtain our results, we rescale the simulations to a common mass, $M_{\rm LG}(< 2.5\,{\rm Mpc}) = 8 \times 10^{12}$ $M_\odot$, which is consistent with current estimates of $M_{\rm LG}(< 1\,{\rm Mpc})$ from the Local Group timing argument (see Section 3.2). We predict that there are 12 ± 3 (68% CL) low-surface-brightness UDGs in the field of the Local Group with stellar masses, $10^6 \leqslant M_*/M_\odot < 10^9$, and effective radii, $R_{\rm e} \geqslant 1.5$ kpc; and as many as 27 ± 5 when selecting UDGs with $R_{\rm e} \geqslant 1$ kpc. The UDGs account for approximately one-quarter and one-half, respectively, of the total population of 52 ± 7 (68% CL) field galaxies with similar stellar masses. As many as 80% of these systems are within 1.5 Mpc of the Milky Way–M31 midpoint and cluster close to these two primary haloes (see Figure 3), in agreement with the results of Fattahi et al. (2020a).

All of the UDGs are as bright as the "classical" satellite galaxies of the Milky Way (i.e., they are brighter than $M_{\rm V} = -8$; see Figure 4); however, they are much more spatially extended and have $R_{\rm e} \geqslant 1.5$ kpc. Therefore they are very diffuse, and have faint effective surface brightnesses that make them difficult to detect against the foreground of Galactic stars and the background of distant galaxies. In the surveys that we consider, we find that the detectability of field UDGs is limited most strongly by their faint effective surface brightness; however, we also find that some field UDGs could be detectable in existing survey data sets and are awaiting discovery by dedicated follow-up searches of archival data (see Figure 4). To estimate how many could be detectable, we generate mock SDSS observations of the field UDG populations in the three highest-resolution HESTIA simulations using survey response functions extrapolated from those described in Koposov et al. (2008). Using these, we predict that there are one to four UDGs detectable in the SDSS footprint (see Figure 5). Almost half of the UDGs that are detected in each mock observation are misclassified as non-UDGs because of projection effects. The total number of UDGs that are detectable is also subject to the variation in the masses of the three Local Group volumes we use. When renormalizing these to $M_{\rm LG}(< 2.5\,{\rm Mpc}) = 8 \times 10^{12}$ $M_\odot$, we find 12 ± 3 field UDGs within 2.5 Mpc of the Milky Way–M31 midpoint, of which 2^{+2}_{-1} are detectable in the footprint of the SDSS (see Section 3.2 and Table 2). A full-sky survey with a response function similar to that of the SDSS, DES, or LSST will detect the entire population of field UDGs.

To generate mock SDSS observations, we used a simple model of the Koposov et al. (2008) SDSS response function. This depends on several physical properties of the galaxies such as their sizes and luminosities, their orientation with respect to the observer, and their physical locations, i.e., their heliocentric distances and projected positions on the sky. The latter are important because galaxies that are partially or totally obscured by the Milky Way can be more difficult to detect against the high-density Galactic stellar foreground, i.e., the ZoA. In HESTIA, we find that 13^{+20}_{-9}% (68% CL) of the total UDG population is in the ZoA on average. We do not account for this when estimating the detection efficiencies of the UDGs, and we further assume that the UDGs do not suffer from dust extinction. Correcting for both of these effects would likely reduce the predicted number of UDGs that are detectable in the surveys.

As we have shown, UDGs are challenging to observe because they are extremely diffuse. However, those that contain large reservoirs of neutral hydrogen, such as most isolated observed UDGs as well as the simulated field UDGs in HESTIA (S. Cardona-Barrero et al. 2023, in preparation), could be detected more easily. In H I surveys the neutral hydrogen could appear as ultracompact high-velocity clouds (UCHVCs; Giovanelli et al. 2009; Adams et al. 2013). Recent searches for UCHVCs and other H I-bright systems using ALFALFA (e.g., Janesh et al. 2019), DES (Tanoglidis et al. 2021), and HIPASS (Zhou et al. 2022) have produced promising results that could expand the catalog of targets for dedicated follow-up studies. Our results suggest that there is a population of low-surface-brightness, spatially extended galaxies in the Local Group awaiting discovery.

Table 2
The Total Number of Field Galaxies, $N_{\rm field,tot}$, UDGs, $N_{\rm UDG,tot}$, and the Number of UDGs Detectable in the SDSS Footprint, $N_{\rm UDG,SDSS}$, for Combinations of $M_{\rm LG}(<2.5$ Mpc) and UDG Selection Criteria

$M_{\rm LG}(<2.5$ Mpc)	$R_{\rm e}$	μ_e (mag	$N_{\rm field,tot}$	$N_{\rm UDG}$			
(10^{12} $M_\odot$)	(kpc)	arcsec^{-2})		Total	SDSS	SDSS+DES	LSST
7	1.0	23.5	45 ± 7	26 ± 5	5^{+4}_{-3}	8 ± 4	8^{+5}_{-3}
7	1.0	24.0	45 ± 7	24 ± 5	4^{+3}_{-2}	7^{+3}_{-4}	7 ± 3
7	1.5	23.5	45 ± 7	13 ± 4	2^{+3}_{-1}	4^{+3}_{-2}	4^{+3}_{-2}
7	1.5	24.0	45 ± 7	10 ± 3	2^{+2}_{-1}	3^{+3}_{-2}	3 ± 2
8	1.0	23.5	52 ± 7	29 ± 5	6^{+4}_{-3}	9 ± 4	9^{+5}_{-4}
8	1.0	24.0	52 ± 7	27 ± 5	5 ± 3	7^{+4}_{-3}	8^{+3}_{-4}
8	1.5	23.5	52 ± 7	15 ± 4	3 ± 2	4^{+3}_{-2}	4^{+3}_{-2}
8	**1.5**	**24.0**	$\mathbf{52 \pm 7}$	$\mathbf{12 \pm 3}$	$\mathbf{2^{+2}_{-1}}$	$\mathbf{3^{+3}_{-2}}$	$\mathbf{4 \pm 2}$
9	1.0	23.5	58 ± 8	33 ± 6	6^{+5}_{-3}	9^{+5}_{-4}	10^{+5}_{-4}
9	1.0	24.0	58 ± 8	30 ± 5	5 ± 3	8 ± 4	8^{+5}_{-3}
9	1.5	23.5	58 ± 8	16 ± 4	3 ± 2	4^{+4}_{-2}	5^{+2}_{-3}
9	1.5	24.0	58 ± 8	13 ± 4	2^{+2}_{-1}	3^{+3}_{-2}	4^{+3}_{-2}

Note. Our fiducial choice is in bold.

The authors thank the anonymous referee for a thoughtful report that improved the manuscript. We also thank Vasily Belokurov, Christopher Conselice, Stefan Gottlöber, and Sergey Pilipenko for useful comments on the draft manuscript, and Steven Gillman for helpful discussions. O.N. and N.I.L. acknowledge support from the Project IDEXLYON at the University of Lyon under the Investments for the Future Program (ANR-16-IDEX-0005) and supplementary support from La Région Auvergne-Rhône-Alpes. O.N. is also supported by the Polish National Science Centre under grant 2020/39/B/ST9/03494. A.D.C. is supported by a Junior Leader fellowship from "La Caixa" Foundation (ID 100010434), code LCF/BQ/PR20/11770010. S.C.B. is supported by the Spanish MINECO under grant SEV-2015-0548-18-3. Y.H. has been partially supported by the Israel Science Foundation grant ISF 1358/18. J.S. acknowledges support from the ANR LOCALIZATION project, grant ANR-21-CE31-0019 of the French Agence Nationale de la Recherche. A.K. is supported by the Ministerio de Ciencia e Innovación (MICINN) under research grant PID2021-122603NB-C21. E. T. acknowledges support by ETAg grant PRG1006 and by the EU through the ERDF CoE grant TK133. The authors acknowledge the Gauss Centre for Supercomputing e.V. (www.Gauss-centre.eu) for providing computing time on the GCS Supercomputer SuperMUC-NG in support of the HESTIA project.

Software: ASTROPY (The Astropy Collaboration et al. 2018), MATPLOTLIB (Hunter 2007), NUMPY (Harris et al. 2020), PYNBODY (Pontzen et al. 2013), PYTHON (Van Rossum & Drake 2009), SCIPY (Virtanen et al. 2020), and NASA's Astrophysics Data System.

Data Availability

A repository of reduced data and scripts to produce the figures in this Letter is available on GitHub [14] and archived in Zenodo (Newton 2023). Requests for access to the raw HESTIA simulation data should be directed to a CLUES Collaboration PI.

[14] Supplementary materials: https://github.com/Musical-Neutron/lg_field_udgs

ORCID iDs

Oliver Newton https://orcid.org/0000-0002-2769-9507
Arianna Di Cintio https://orcid.org/0000-0002-9856-1943
Salvador Cardona–Barrero https://orcid.org/0000-0002-9990-4055
Noam I. Libeskind https://orcid.org/0000-0002-6406-0016
Alexander Knebe https://orcid.org/0000-0003-4066-8307
Jenny G. Sorce https://orcid.org/0000-0002-2307-2432
Matthias Steinmetz https://orcid.org/0000-0001-6516-7459
Elmo Tempel https://orcid.org/0000-0002-5249-7018

References

Abbott, T. M. C., Abdalla, F. B., Allam, S., et al. 2018, ApJS, 239, 18
Adams, E. A. K., Giovanelli, R., & Haynes, M. P. 2013, ApJ, 768, 77
Amorisco, N. C., & Loeb, A. 2016, MNRAS, 459, L51
Bechtol, K., Drlica-Wagner, A., Balbinot, E., et al. 2015, ApJ, 807, 50
Benavides, J. A., Sales, L. V., Abadi, M. G., et al. 2021, NatAs, 5, 1255
Blanton, M. R., Bershady, M. A., Abolfathi, B., et al. 2017, AJ, 154, 28
Bruzual, G., & Charlot, S. 2003, MNRAS, 344, 1000
Caldwell, N., Walker, M. G., Mateo, M., et al. 2017, ApJ, 839, 20
Cardona-Barrero, S., Di Cintio, A., Battaglia, G., Macciò, A. V., & Taibi, S. 2023, MNRAS, 519, 1545
Carlesi, E., Hoffman, Y., & Libeskind, N. I. 2022, MNRAS, 513, 2385
Carleton, T., Errani, R., Cooper, M., et al. 2019, MNRAS, 485, 382
Chabrier, G. 2003, PASP, 115, 763
Chan, T. K., Kereš, D., Wetzel, A., et al. 2018, MNRAS, 478, 906
Collins, M. L. M., Chapman, S. C., Rich, R. M., et al. 2013, ApJ, 768, 172
Conselice, C. J., Iii, J. S. G., & Wyse, R. F. G. 2003, AJ, 125, 66
De Rijcke, S., Penny, S. J., Conselice, C. J., Valcke, S., & Held, E. V. 2009, MNRAS, 393, 798
Di Cintio, A., Brook, C. B., Dutton, A. A., et al. 2017, MNRAS, 466, L1
Diemer, B. 2021, ApJ, 909, 112
Doumler, T., Hoffman, Y., Courtois, H., & Gottlöber, S. 2013, MNRAS, 430, 888
Drlica-Wagner, A., Bechtol, K., Mau, S., et al. 2020, ApJ, 893, 47
Drlica-Wagner, A., Bechtol, K., Rykoff, E. S., et al. 2015, ApJ, 813, 109
Fattahi, A., Deason, A. J., Frenk, C. S., et al. 2020b, MNRAS, 497, 4459
Fattahi, A., Navarro, J. F., & Frenk, C. S. 2020a, MNRAS, 493, 2596
Garling, C. T., Peter, A. H. G., Kochanek, C. S., Sand, D. J., & Crnojević, D. 2020, MNRAS, 492, 1713

Garrison-Kimmel, S., Boylan-Kolchin, M., Bullock, J. S., & Lee, K. 2014, MNRAS, 438, 2578
Gill, S. P. D., Knebe, A., & Gibson, B. K. 2004, MNRAS, 351, 399
Giovanelli, R., Haynes, M. P., Kent, B. R., & Adams, E. A. K. 2009, ApJL, 708, L22
Grand, R. J. J., Gómez, F. A., Marinacci, F., et al. 2017, MNRAS, 467, 179
Harris, C. R., Millman, K. J., van der Walt, S. J., et al. 2020, Natur, 585, 357
Hartl, O. V., & Strigari, L. E. 2022, MNRAS, 511, 6193
Hoffman, Y., & Ribak, E. 1991, ApJL, 380, L5
Hunter, J. D. 2007, CSE, 9, 90
Impey, C., Bothun, G., & Malin, D. 1988, AJ, 330, 634
Janesh, W., Rhode, K. L., Salzer, J. J., et al. 2019, AJ, 157, 183
Jerjen, H., Binggeli, B., & Freeman, K. C. 2000, AJ, 119, 593
Jiang, F., Dekel, A., Freundlich, J., et al. 2019, MNRAS, 487, 5272
Ivezić, Ž., Kahn, S. M., Tyson, J. A., et al. 2019, ApJ, 873, 111
Karakas, A. I. 2010, MNRAS, 403, 1413
Kirby, E. N., Bullock, J. S., Boylan-Kolchin, M., Kaplinghat, M., & Cohen, J. G. 2014, MNRAS, 439, 1015
Knollmann, S. R., & Knebe, A. 2009, ApJS, 182, 608
Koda, J., Yagi, M., Yamanoi, H., & Komiyama, Y. 2015, ApJL, 807, L2
Koposov, S., Belokurov, V., Evans, N. W., et al. 2008, ApJ, 686, 279
Laine, S., Martinez-Delgado, D., Trujillo, I., et al. 2018, LSST Cadence Optimization White Paper in Support of Observations of Unresolved Tidal Stellar Streams in Galaxies beyond the Local Group, arXiv:1812.04897
Leisman, L., Haynes, M. P., Janowiecki, S., et al. 2017, ApJ, 842, 133
Lemos, P., Jeffrey, N., Whiteway, L., et al. 2021, PhRvD, 103, 023009
Libeskind, N. I., Carlesi, E., Grand, R. J. J., et al. 2020, MNRAS, 498, 2968
Martínez-Delgado, D., Läsker, R., Sharina, M., et al. 2016, AJ, 151, 96
McConnachie, A. W. 2012, AJ, 144, 4
Mieske, S., Hilker, M., Infante, L., & de Oliveira, C. M. 2007, A&A, 463, 503
Nadler, E. O., Mao, Y.-Y., Green, G. M., & Wechsler, R. H. 2019, ApJ, 873, 34
Newton, O. 2023, Musical-Neutron/lg_field_udgs: HESTIA Local Group field UDG paper scripts & reduced data, v1.1, Zenodo, doi:10.5281/zenodo.7757685
Newton, O., Cautun, M., Jenkins, A., Frenk, C. S., & Helly, J. C. 2018, MNRAS, 479, 2853
Penny, S. J., Conselice, C. J., De Rijcke, S., & Held, E. V. 2009, MNRAS, 393, 1054
Pontzen, A., Roškar, R., Stinson, G., & Woods, R. 2013, pynbody: N-Body/SPH analysis for python, Astrophysics Source Code Library, ascl:1305.002
Portinari, L., Chiosi, C., & Bressan, A. 1998, A&A, 334, 505
Planck Collaboration, Ade, P. A. R., Aghanim, N., et al. 2014, A&A, 571, A16
Román, J., & Trujillo, I. 2017, MNRAS, 468, 703
Sandage, A., & Binggeli, B. 1984, AJ, 89, 919
Sorce, J. G., Gottlöber, S., Yepes, G., et al. 2016, MNRAS, 455, 2078
Springel, V. 2010, MNRAS, 401, 791
Tanoglidis, D., Drlica-Wagner, A., Wei, K., et al. 2021, ApJS, 252, 18
The Astropy Collaboration, Price-Whelan, a. A. M., Sipőcz, B. M., et al. 2018, AJ, 156, 123
Thompson, L. A., & Gregory, S. A. 1993, AJ, 106, 2197
Torrealba, G., Koposov, S. E., Belokurov, V., & Irwin, M. 2016, MNRAS, 459, 2370
Tremmel, M., Wright, A. C., Brooks, A. M., et al. 2020, MNRAS, 497, 2786
Trujillo, I., Roman, J., Filho, M., & Almeida, J. S. 2017, ApJ, 836, 191
Tully, R. B., Courtois, H. M., Dolphin, A. E., et al. 2013, AJ, 146, 86
van Dokkum, P. G., Abraham, R., Merritt, A., et al. 2015, ApJL, 798, L45
Van Rossum, G., & Drake, F. L. 2009, Python 3 Reference Manual (Scotts Valley, CA: CreateSpace)
Virtanen, P., Gommers, R., Oliphant, T. E., et al. 2020, NatMe, 17, 261
Walsh, S. M., Willman, B., & Jerjen, H. 2009, AJ, 137, 450
Wright, A. C., Tremmel, M., Brooks, A. M., et al. 2021, MNRAS, 502, 5370
Zhou, Y.-F., Sengupta, C., Chandola, Y., et al. 2022, MNRAS, 516, 1781